Tests of collision operators using laboratory measurements of shear Alfvén wave dispersion and damping

D. J. Thuecks,* C. A. Kletzing, F. Skiff, and S. R. Bounds
Department of Physics and Astronomy, University of Iowa, 203 Van Allen Hall, Iowa City, Iowa 52242

S. Vincena
Department of Physics, University of California at Los Angeles, Los Angeles, California 90095-1696
(Dated: April 30, 2009)

Measurements of shear Alfvén waves are used to test the predictions of a variety of different electron collision operators, including several Krook collision operators as well as a Lorentz collision operator. New expressions for the collisional warm-plasma dielectric tensor resulting from the use of the fully-magnetized collisional Boltzmann equation are presented here. Theoretical predictions for the parallel phase velocity and damping as a function of perpendicular wave number $k_\perp$ are derived from the dielectric tensor. Laboratory measurements of the parallel phase velocity and damping of shear Alfvén waves were made to test these theoretical predictions in both the kinetic ($v_{te} \gg v_A$) and inertial ($v_{te} \ll v_A$) parameter regimes and at several wave frequencies ($\omega < \omega_{ci}$). Results show that in the inertial regime, the best match between measurements and theory occur when any of the Krook operators are used to describe electron collisions. In contrast, the best agreement in the kinetic regime is found when collisions are completely ignored.

PACS numbers: 52.35.Hr, 52.20.Fs, 52.72.+v

I. INTRODUCTION

A difficult problem that often arises when trying to derive theoretical predictions for the behavior of waves in a plasma is how to include effects of particle collisions in the theory. In the limit of very low collisionality, one can typically ignore the effects of collisions completely. In the limit of very high collisionality, a fluid approach such as that developed by Braginskii[1] can be used to describe wave behavior. It is the case of intermediate collisionality that bridges these two extremes where the problem of how to account for collisions must be addressed.

Some of the first researchers to try to bridge the divide between the very high and very low collisionality were Bhatnagar, Gross, and Krook. In a series of papers[2–4], they developed a set of collisional operators that could be introduced in the Boltzmann equation. These collisional operators will be referred to as Krook operators for the remainder of this paper (though they can also often be referred to as BGK collision operators). Several collision operators of varying complexity were constructed in these papers, each type distinguished from the others by which conservation properties it conserves instantaneously (number of particles, energy, or none at all). Although these operators represent a crude attempt to include the effects of collisionality in the Boltzmann equation, they are still one of the few analytically tractable methods of describing collisional effects. Due to the crudeness of the operators, one may initially expect results arising from the inclusion of Krook operators to provide only a qualitative description of wave behavior, but in fact, these operators often provide very good quantitative descriptions of wave behavior.

We will develop theoretical predictions for the behavior of shear Alfvén waves including kinetic effects and electron collisional effects by including Krook collision operators in a warm-plasma derivation. We then test these predictions by comparing them to experimental results. Earlier treatments of Krook collision operators (a nice summary of which is given by Opher et al.[5]) and their applicability to the current experiment is discussed. As we will detail later, many of the earlier treatments of Krook collisions (specifically the number- and energy-conserving operators) derived results using assumptions that are not appropriate to this current experiment. Additionally, while several authors[5–7] have compared predictions of these models to each other and to other computational models, few have compared these predictions to experimental data.

In this paper, we present the results of experiments conducted using the LArge Plasma Device (LAPD)[8] at the University of California at Los Angeles (UCLA) that measured the parallel phase velocity and damping rates as a function of perpendicular wave number $k_\perp$ for the kinetic ($v_{te} > v_A$) and inertial ($v_{te} < v_A$) regimes. These experimental results are directly compared to theoretical curves including the effects of electron collisions, allowing us to perform sensitive tests of the accuracy of these operators. We will begin with a description of shear Alfvén waves in Section II. Described in Section III, the electron collisions are modeled using several different Krook collision operators of varying complexity as well as pitch-angle scattering described by a Lorentz collision operator. Section IV will include a description of the experiment whose results will then be matched to our theoretical predicions. The results of these comparisons will be presented and discussed in Sections V and VI.

II. SHEAR ALFVÉN WAVES

Alfvén waves were first predicted by Hannes Alfvén[9] in 1942. Using basic magnetohydrodynamic (MHD) equations, he derived the dispersion equation for an "ideal" Alfvén wave, $\omega = v_A k_{||}$, where $v_A = B_0/\sqrt{\mu_0 n_i m_i}$, B_0 is the background magnetic field, $k_{||}$ is the component of the wave number parallel to the background magnetic field, and n_i and m_i are the

ion density and mass. The Alfvén wave is an electromagnetic wave that exists at frequencies for which $\omega < \omega_{ci}$. In the MHD approximation, the Alfvén wave can only transport energy along the magnetic field since the group velocity is along the magnetic field. It can be shown that the electric and magnetic fields of the wave are always perpendicular to the background magnetic field which is in stark contrast to the Alfvén wave when kinetic effects are included.

Early attempts to include particle kinetic effects into a description of the Alfvén wave were discussed by Stéfant[10], Hasegawa[11], and Goertz and Boswell[12]. For the purposes of this paper, we will use the term shear Alfvén waves to refer to Alfvén waves including particle kinetic effects. These papers showed that the shear Alfvén wave can be separated into two regimes, characterized by the ratio of v_{te}/v_A where $v_{te} = \sqrt{T_e/m_e}$ is the electron thermal speed (T_e is in units of Joules unless otherwise stated) and v_A is the MHD Alfvén velocity given above. In the kinetic regime, $v_{te} \gg v_A$ and $2m_e/m_i < \beta < 1$ where $\beta = 2(m_e/m_i)(v_{te}/v_A)^2$. This regime is applicable in the magnetosphere beyond approximately 5 Earth radii and in the solar wind. The necessary ratio is typically achieved in a laboratory plasma with high density, high electron temperature, and low magnetic field. This is the situation that is discussed by Hasegawa[11] where he uses two-fluid theory to derive a dispersion relation for the kinetic Alfvén wave

$$\frac{\omega}{k_{||}} = v_A\sqrt{1 + k_\perp^2\rho_s^2} \tag{1}$$

where $k_\perp$ is the component of the wave number perpendicular to the background magnetic field, $\rho_s = C_s/\omega_{ci}$ is the ion acoustic gyroradius, $C_s = \sqrt{T_e/m_i}$ is the ion acoustic speed, and ω_{ci} is the ion cyclotron frequency. For small values of $k_\perp$, the dispersion relation is the same as the MHD case. As the perpendicular spatial structure of the kinetic Alfvén wave decreases and approaches ρ_s (so that $k_\perp\rho_s \sim 1$), kinetic effects become important and the parallel phase velocity increases above v_A.

In the inertial regime, $v_{te} \ll v_A$ so that $\beta < 2m_e/m_i$, which is satisfied in the ionosphere and out to 4-5 Earth radii. In the laboratory, this regime is achieved in a plasma with low density, low electron temperature, and high magnetic field. Goertz and Boswell[12] derived a two-fluid expression for the dispersion relation of the inertial Alfvén wave given as

$$\frac{\omega}{k_{||}} = v_A\frac{1}{\sqrt{1 + k_\perp^2\delta_e^2}}. \tag{2}$$

In the inertial regime, particle kinetic effects become important as the perpendicular spatial structure of the inertial Alfvén wave decreases and approaches the electron skin depth $\delta_e = c/\omega_{pe}$ where ω_{pe} is the electron plasma frequency. Just as in the kinetic regime, the parallel phase velocity of the inertial Alfvén wave is v_A for small $k_\perp$ values. Unlike in the kinetic regime, the parallel phase velocity decreases as $k_\perp$ increases.

Unlike in the MHD derivation, the inclusion of particle kinetic effects leads to a component of the wave electric field that is parallel to the background magnetic field. The ability of the parallel electric field component of the shear Alfvén wave to accelerate charged particles along the magnetic field is thought to play an important role in the magnetosphere-ionosphere system, specifically in auroral electron acceleration.[12,13]

Many authors have derived theoretical dispersion relations for the shear Alfvén wave and studied laboratory and space physics applications where shear Alfvén waves play an important role. Even so, there have been few detailed experimental verifications of the dispersion relation in the laboratory. Several Australian researchers were among the first to study the behavior of Alfvén waves with small perpendicular structure in linear[14] and toroidal[15] geometries. More recently, groups at UCLA have conducted experiments in the LAPD to measure the dispersion relation and related properties of shear Alfvén waves.[16–19] In these experiments, shear Alfvén waves were launched by a small-disk antenna that emitted a wave with power distributed over a broad range of values of $k_\perp$, though the size of the disks were chosen to give some preference to scale sizes near δ_e. The wave was measured at several different axial positions in order to determine the evolution of the radial profile of the wave, and then this radial profile was compared to a theory derived by Morales et al.[20,21]

III. THEORY

Previous experience of the UCLA group has shown that electron collisional effects tend to be important in accurately describing the dynamics of the shear Alfvén wave in the LAPD. In fact, under our experimental conditions, the electron collision frequency is $\nu_e = 1.4$ MHz in the kinetic regime and $\nu_e = 7.0$ MHz in the inertial regime, where the electron collision frequency

$$\nu_e = \frac{4\sqrt{2\pi}e^4 Z n_0 \ln\Lambda}{3m_e^2 v_{te}^3} \approx 2.9\times10^{-6}\frac{Z n_0 \ln\Lambda}{T_e^{3/2}} \tag{3}$$

has been taken from Braginskii[1] and is a characteristic electron collision frequency including effects due to collisions with ions as well as other electrons. In this expression, $Z = 1$ for singly-ionized helium, and T_e is in units of eV. This results in values of ν_e/ω ranging from 10 to 20 in the kinetic regime and 18 to 28 in the inertial regime. Thus, we can investigate a variety of different electron collision operators $(\partial f_e/\partial t)_c$ to determine which, if any, show adequate agreement with data.

A. Warm plasma theory, no collisions

In order to test the effects of various electron collision operators, warm plasma theory for Alfvén waves is developed here. This theory includes important particle kinetic effects in the determination of the theoretical phase velocity in addition to providing a theoretical prediction for the damping rate, which, in general, tends to be dominated by Landau damping and electron collisions in the LAPD. Electron-ion collisional

effects were included via a collision operator in the electron Boltzmann equation

$$\frac{\partial f_e}{\partial t} + \mathbf{v}\cdot\nabla f_e + \frac{q_e}{m_e}\left[\mathbf{E}+\mathbf{v}\times\mathbf{B}\right]\cdot\nabla_v f_e = \left(\frac{\partial f_e}{\partial t}\right)_c \quad (4)$$

where the electron distribution function is $f_e(\mathbf{x},\mathbf{v},t) = f_{e0}(\mathbf{v}) + f_{e1}(\mathbf{x},\mathbf{v},t)$ and f_{e0} is an equilibrium distribution function (it is assumed to be a Maxwellian distribution in our derivations).

The wave equation is given by

$$\mathbf{k}\times(\mathbf{k}\times\mathbf{E}) + \frac{\omega^2}{c^2}\boldsymbol{\varepsilon}\cdot\mathbf{E} = 0 \quad (5)$$

where $\boldsymbol{\varepsilon} = \mathbf{1} + \boldsymbol{\varepsilon}_e + \boldsymbol{\varepsilon}_i$ is the warm plasma dielectric tensor. Initially, collisions will be assumed to be unimportant, so that $(\partial f_e/\partial t)_c = 0$. Under this assumption, $\boldsymbol{\varepsilon}$ has been derived in many texts (e.g. Swanson[22]), so the full tensor will not be given here. In the low frequency limit ($\omega \ll \omega_{ci}$), equation 5 can be reduced to

$$(n_{||}^2 - \varepsilon_{xx})\varepsilon_{zz} + n_\perp^2\varepsilon_{xx} = 0 \quad (6)$$

where $n_{||} = ck_{||}/\omega$, $n_\perp = ck_\perp/\omega$, and the relevant $\boldsymbol{\varepsilon}$ tensor elements are given as

$$\begin{aligned}\varepsilon_{xx} &= 1 + \sum_j \frac{\omega_{pj}^2}{\sqrt{2}\omega k_{||} v_{tj}}\frac{1}{\mu_j}\sum_{n=-\infty}^{\infty} n^2\Gamma_n(\mu_j)Z(\zeta_{nj}) \\ &\approx \frac{\omega_{pi}^2}{\omega_{ci}^2-\omega^2}\frac{1-\Gamma_0(\mu_i)}{\mu_i}\end{aligned} \quad (7)$$

$$\begin{aligned}\varepsilon_{zz} &= 1 - \sum_j \frac{\omega_{pj}^2}{\sqrt{2}\omega k_{||} v_{tj}}\sum_{n=-\infty}^{\infty}\Gamma_n(\mu_j)\zeta_{nj}Z'(\zeta_{nj}) \\ &\approx 2\frac{\omega_{pe}^2}{\sqrt{2}\omega k_{||} v_{te}}\zeta_{0e}[1+\zeta_{0e}Z(\zeta_{0e})].\end{aligned} \quad (8)$$

The approximations given in Equations 7 and 8 have been given previously by Gekelman et al.[16] and result from the assumptions that $\omega \ll \omega_{ce}$, $\omega \ll n\omega_{ci}$ when $n > 1$, and $\mu_e \ll 1$ so that $\Gamma_0(\mu_e) \approx 1$ and $\Gamma_n(\mu_e) \approx 0$ when $n \neq 0$. In these equations, j represents species (e for electrons, i for ions), $\mu_j = k_\perp^2\rho_j^2$, ρ_j is the particle gyroradius, $\Gamma_n(\mu_j) = e^{-\mu_j}I_n(\mu_j)$, $I_n(x)$ is the modified Bessel function, $\zeta_{nj} = (\omega - n\omega_{cj})/(\sqrt{2}k_{||}v_{tj})$, $Z(\zeta_{nj})$ is the plasma dispersion function[23], and $Z'(\zeta_{nj}) = -2[1+\zeta_{nj}Z(\zeta_{nj})]$ is the derivative of the plasma dispersion function with respect to ζ_{nj}. From these equations, the following approximate dispersion relation can be derived:

$$Z'(\zeta_{0e})\left[\frac{v_A^2}{v_{te}^2}\frac{1-(\omega^2/\omega_{ci}^2)\mu_i}{1-\Gamma_0(\mu_i)} - \zeta_{0e}^2\right] = \frac{c^2k_\perp^2}{\omega^2}. \quad (9)$$

Finite-Larmor radius effects are incorporated through the term $1-\Gamma_0(\mu_i)$. As the perpendicular scale of the electric field approaches and becomes smaller than the size of the ion gyroradius (or, as μ_i approaches and exceeds 1), this term accounts for a reduction in the electric field that an ion experiences from the value at the guiding center to an average over the whole Larmor orbit[24]. The finite-frequency effects are included via the $1-\omega^2/\omega_{ci}^2$ term. When $\omega \ll \omega_{ci}$, this term approaches unity. As $\omega \to \omega_{ci}$, the wave dynamics significantly disrupt the ion cyclotron motion.

B. Krook collisions

The Krook collision operators represent a simplified attempt to model particle collisions and their effect on the wave dynamics. Instead of focussing on the dynamics of individual collisions, the operators instead represent an assumption that collisions will drive a slightly non-Maxwellian electron distribution f_e back to a Maxwellian distribution f_{e0} in a time on the order of $1/\nu(v)$ where $f_e = f_{e0} + f_{e1}$ and $\nu(v)$ is a velocity dependent collision frequency. The relaxation rate is often approximated using a velocity-independent collision frequency, ν_e (in the case of electron collisions), and our derivations will be no different. These approximations allow us to derive the collisional dielectric tensor using the same method as was used in the collisionless case (i.e. the same as in Swanson[22]) with only minor modifications to the procedure. As such, the derivations will not be presented here, but only the relevant results will be given. It is important to note that while these approximations greatly simplify the derivation of the wave dispersion relations from the Boltzmann equation (as compared with a full Fokker-Planck collision integral), the resulting collision operators are not able to properly describe all of the collisional effects. In many cases, however, it can provide at least a semi-quantitative view of the effects of collisions on wave propagation and damping with varying degrees of success.

The simplest type of Krook collision operator, and the one that is most often used in analytic derivations, is a non-conserving Krook operator[2]

$$\begin{aligned}\left(\frac{\partial f_e}{\partial t}\right)_c &= -\nu_e(f_e - f_{e0}) \\ &= -\nu_e f_{e1}.\end{aligned} \quad (10)$$

This represents the idea that in a collision, electrons are absorbed based on the current distribution f_e and re-emitted based on the background Maxwellian distribution f_{e0}, leading to the number of particles being conserved only when averaging over a disturbance cycle (the time scale over which the fluctuating density component varies).

Since ions are far more massive than electrons, to a first approximation only the electron terms of the dielectric tensor $\boldsymbol{\varepsilon}_e$ are modified by electron collisions where $\boldsymbol{\varepsilon} = \mathbf{1} + \boldsymbol{\varepsilon}_e + \boldsymbol{\varepsilon}_i$. The resulting electron dielectric tensor $(\boldsymbol{\varepsilon}_e)_{NC}$ has the same form as in the collisionless case, but all elements in the electron dielectric tensor are modified so that $\zeta_{ne} \to \xi_{ne}$ where $\xi_{ne} = (\eta\omega - n\omega_{ce})/(\sqrt{2}k_{||}v_{te})$, $\eta = 1 + i\nu_e/\omega$, and the derivative of the plasma dispersion function is now in terms of ξ_{ne}. This is not the same as just changing $\omega \to \omega + i\nu_e$ as is often stated for cold-plasma theory, as there are factors of ω

arising from Maxwell's equations that should not be modified by the Krook collision operator. In fact, the same is true even in cold plasma theory, where it is typically more accurate to use the shortcut $m_e \rightarrow m_e(1+i\nu_e/\omega)$. Just as in the collisionless case, the wave dynamics are approximately governed by Equation 6 where the parallel dielectric tensor in Equation 8 is modified to become

$$(\varepsilon_{zz})_{NC} = 1 - \sum_j \frac{\omega_{pj}^2}{\sqrt{2}\omega k_{||} v_{tj}} \sum_{n=-\infty}^{\infty} \Gamma_n(\mu_j)\xi_{nj} Z'(\xi_{nj}) \tag{11}$$

$$\approx 2\frac{\omega_{pe}^2}{\sqrt{2}\omega k_{||} v_{te}} \xi_{0e}[1 + \xi_{0e} Z(\xi_{0e})]. \tag{12}$$

This approximate expression for the parallel dielectric tensor agrees with that given by Vincena et al.[19] The non-conserving Krook model has the virtue of ease of use, but suffers in that it does not satisfy conservation laws for the number of particles, momentum, or energy.

As noted, the Krook model above only conserves the number of particles when averaged over a disturbance cycle. Instantaneous conservation of particle number can be included through a relatively minor modification to the non-conserving collision operator[3] so that

$$\begin{aligned}\left(\frac{\partial f_e}{\partial t}\right)_c &= -\nu_e \left(f_e - \frac{n(x,t)}{n_0} f_{e0}\right) \\ &= -\nu_e \left(f_{e1} - \frac{f_{e0}}{n_0}\int d^3u f_{e1}\right)\end{aligned} \tag{13}$$

where $n(x,t) = \int d^3v f_e(v) = n_0 + n_1$, n_0 is the equilibrium density, and n_1 is the fluctuating density component. In this case, electrons with velocities between $\mathbf{v}$ and $\mathbf{v} + d\mathbf{v}$ are absorbed based on the current distribution function f_e and re-emitted with a velocity distribution governed by f_{e0} (just as above), but now the re-emission rate is proportional to the fluctuating density $n(x,t)$. The resulting modified dielectric tensor is given by

$$\begin{aligned}(\boldsymbol{\varepsilon}_e)_{num} &= (\boldsymbol{\varepsilon}_e)_{NC} \\ &- \frac{i\nu}{\omega}\frac{\omega_{pe}^2}{\omega_{ce}^2}\frac{\mathbf{G}_{e+}\mathbf{G}_{e-}}{2k_z^2}\left[1 + \gamma \sum_{n=-\infty}^{\infty} \Gamma_n(\mu_e) Z(\xi_{ne})\right]^{-1}\end{aligned} \tag{14}$$

where $\mathbf{G}_{e+}\mathbf{G}_{e-}$ is the outer product of two vectors defined by the expression

$$\begin{aligned}\mathbf{G}_{s\pm} = &\left[k_x \sum_{n=-\infty}^{\infty} \frac{n\Gamma_n(\mu_s)}{\mu_s} Z_0(\xi_{ns})\right]\hat{x} \\ &\pm \left[ik_x \frac{q_s}{|q_s|} \sum_{n=-\infty}^{\infty} \Gamma'_n(\mu_s) Z_0(\xi_{ns})\right]\hat{y} \\ &+ \left[\frac{\omega_{ce}}{\sqrt{2}v_{te}} \sum_{n=-\infty}^{\infty} \Gamma_n(\mu_s) Z'(\xi_{ns})\right]\hat{z}\end{aligned} \tag{15}$$

and $\gamma = i\nu_e/(\sqrt{2}k_{||}v_{te})$. The analog to the approximation in Equation 8 is then given by

$$(\varepsilon_{zz})_{num} \approx 2\frac{\omega_{pe}^2}{\sqrt{2}\omega k_{||} v_{te}} \zeta_{0e} \frac{1 + \xi_{0e} Z(\xi_{0e})}{1 + \gamma Z(\xi_{0e})}. \tag{16}$$

Neither of the two models above provide a description of energy-conserving collisions. In their 1954 paper, Bhatnagar et al.[3] extended the previous models to account for energy conservation (in addition to conserving particle number). The energy-conserving collision operator is given by

$$\begin{aligned}\left(\frac{\partial f_e}{\partial t}\right)_c &= -\frac{n}{\sigma} f_e + \frac{n^2}{\sigma} F_{e0} \\ &= -\nu_e \Bigg[f_{e1} - \frac{f_{e0}}{n_0}\int d^3u f_{e1} \\ &- \frac{f_{e0}}{2n_0}\left(\frac{v^2}{3v_{te}^2} - 1\right)\int d^3u \left(\frac{u^2}{v_{te}^2} - 3\right) f_{e1}\Bigg]\end{aligned} \tag{17}$$

where $n_0/\sigma = \nu_e$, and F_{e0} has the form of a Maxwellian distribution, but instead of using a constant temperature $T_e = T_{e0}$ (as we had up until this point), we instead allow the temperature to vary so that $T_e(\mathbf{x},t) = T_{e0} + T_{e1}(\mathbf{x},t)$. In this case, electrons with velocities between $\mathbf{v}$ and $\mathbf{v} + d\mathbf{v}$ are absorbed based on the distribution f_e and at a rate proportional to $n(\mathbf{x},t)$, and are then re-emitted based on the distribution F_e and at a rate proportional to n^2.

It is possible, though tedious, to derive an expression for ε_{zze} from the Boltzmann equation, again following the method used in the previous two cases. An expression for the full dielectric tensor is far too complicated to be useful to reproduce here, although a relatively compact approximation to ε_{zze} can be given (using the same approximations used to produce Equation 8). In this case, the new dielectric tensor element is given approximately as

$$(\varepsilon_{zz})_{energy} \approx 2\frac{\omega_{pe}^2}{\sqrt{2}\omega k_{||} v_{te}}\left[Z_2 - \frac{2}{3}\gamma \frac{\frac{7}{4}Z_1^2 - Z_1 Z_3 + Z_3^2 + \gamma\left(Z_0 Z_1^2 - 2Z_1 Z_2 Z_3 + Z_1^2 Z_4 + Z_0 Z_3^2\right)}{1 + \frac{2}{3}\gamma\left(\frac{11}{4}Z_0 - Z_2 + Z_4\right) + \frac{2}{3}\gamma^2\left(Z_0^2 - Z_2^2 + Z_0 Z_4\right)}\right] \tag{18}$$

where we let

$$Z_n = \frac{1}{\sqrt{\pi}}\int_{-\infty}^{\infty} \frac{u^n e^{-u^2}}{u - \xi_{0e}} du. \tag{19}$$

The expressions for the number-conserving dielectric tensor given by Equation 14 and for the energy-conserving di-

electric tensor element given by Equation 18 have not been previously published to our knowledge. Other authors have treated these collision operators, but often assuming conditions that are not appropriate to our experiments. For example, Clemmow and Dougherty[25] and Fried et al.[26] treated the non-conserving and energy-conserving Krook operators respectively and derived scalar dielectric susceptibilities in the case of no background magnetic field, a case which is inconsistent with the description of an Alfvén wave. Alexandrov et al.[27] also addressed the number-conserving Krook operator and derived an expression for the full warm-plasma dielectric tensor assuming a background magnetic field. His expressions for the dielectric tensor nearly agree with the expressions given in this paper. There are differences in the sign of the off-diagonal elements of the collisionless dielectric tensor, and the ε_{zz} term of the collisionless dielectric tensor given by Alexandrov et al.[27] appears to contain a typographical error, but we have no independent verification of this from other sources. Additionally, in order for his expression for the number-conserving dielectric tensor to match the expression presented here, what he calls the particle species contribution to the collisionless dielectric tensor ($\varepsilon^{\alpha}_{\text{Alexandrov}}$) can be related to what we call the collisionless particle species contribution (ε_{α}) by the expression $\varepsilon^{\alpha}_{\text{Alexandrov}} = \mathbf{1} + \varepsilon_{\alpha}$ where $\varepsilon = \mathbf{1} + \varepsilon_e + \varepsilon_i$ is our expression for the complete collisionless dielectric tensor. Rewoldt et al.[6] treated all of the Krook operators discussed in this paper, though he made use of a gyrokinetic approach to derive scalar dielectric susceptibilities. Since his resulting scalar dielectric susceptibility for the non-conserving Krook operator does not agree with the expression given by Equation 11, there is no reason to believe that the scalar susceptibilities he gives for the other two Krook operators should be appropriate for our experiment.

C. Pitch-angle scattering

One of the main disadvantages of the above models is that they do not incorporate a velocity-dependent collision frequency. The Lorentz (or pitch-angle) collision operator[28] represents an attempt to overcome this deficiency. The collision operator represents electron-ion collisions as a series of elastic binary collisions where the electron's direction, but not the magnitude of the electron's velocity, is changed in a collision with a stationary ion. The Lorentz collision operator is given by

$$\left(\frac{\partial f_e}{\partial t}\right)_c = -\nu(v)\frac{\partial}{\partial \mu}\left[(1-\mu^2)\frac{\partial f_{e1}}{\partial \mu}\right] \tag{20}$$

where $v_z = v\mu$. As this operator describes electron-ion collisions only, we must use $\nu(v) = -\nu_{ei}(\sqrt{2}v_{te}/v)^3$ where

$$\nu_{ei} = \frac{2\pi n_0 e^4 \ln\Lambda}{m_e^2(\sqrt{2}v_{te})^3} \approx 1.9\times 10^{-6}\frac{n_0 \ln\Lambda}{T_e^{3/2}} \tag{21}$$

has been taken from Peñano et al.[29] (T_e is in units of eV for this expression).

Equation 20 leads to the parallel dielectric tensor element

$$\varepsilon_{zz} = -\frac{\omega_{pe}^2}{\sqrt{2}\omega k_{||} v_{te}}\zeta_{0e} Z_P(\zeta_{0e}) \tag{22}$$

where the function $Z_P(\zeta_{0e})$ is derived by Peñano et al.[29] and is given by the following equations:

$$Z_P(\zeta_{0e}) = -\int_0^{\infty} \frac{(8/\sqrt{\pi})t^7 exp(-t^2)dt}{t^5 - 3\zeta_{0e}^2 t^3 - 6\gamma_{ei}\zeta_{0e} + 6\zeta_{0e}t^4(a_2/a_1)/5} \tag{23}$$

$$\frac{a_n}{a_{n-1}} = \frac{-b_n}{d_n + b_{n+1}(a_{n+1}/a_n)} \tag{24}$$

$$b_n = i\frac{nt^4}{(2n-1)(2n+1)}, d_n = -i\frac{\zeta_{0e}t^3 + \gamma_{ei}n(n+1)}{2n+1} \tag{25}$$

where $\gamma_{ei} = i\nu_{ei}/(\sqrt{2}k_{||}v_{te})$. The Lorentz collision operator is similar to the energy-conserving Krook operator in that it simultaneously conserves particle number, momentum, and energy. Unlike the Krook operators above which relax the electron distribution function to a Maxwellian form, the Lorentz operator causes the electron distribution function to relax to a form that is isotropic with respect to the ions.[30] The Lorentz collision operator does have some drawbacks, however. First, in the limit of low collisionality, the convergence of the continued fraction a_2/a_1 is very slow and must be carried out to very high n. Also, as Opher et al.[5] points out, Peñano's derivation of the $Z_P(\zeta)$ function was performed for the case of instabilities where the wave grows with time, and that it has not been rigorously shown that this same function is valid for damping problems (such as the experiments presented in this paper).

IV. EXPERIMENT

A. LAPD

The LAPD is a cylindrical device in which a discharge plasma is produced that is approximately 40 cm in diameter and 16 m in length. The plasma discharges have a duration on the order of 10 ms, and a repetition rate of 1 Hz. Experiments were performed using a helium plasma in which a uniform axial ($\hat{\mathbf{z}}$) magnetic field was applied. Electron density and temperature measurements were made using a swept Langmuir probe, with the density then scaled to match measurements from a microwave interferometer.

While operating in the kinetic regime, an axial magnetic field of 600 G was applied. Experiments were conducted in the "flat top" of the discharge when the density and temperature were relatively high. Results from Langmuir probe measurements showed the resulting plasma had an electron

density of 1.1×10^{12} cm^{-3}, and an electron temperature of 8.0 eV. Although the Langmuir probe density measurement was scaled to a line-integrated measurement from a microwave interferometer, our results showed a need to reduce the scaled density by 14% (in both the kinetic and inertial regimes), resulting in a density of 9.5×10^{11} cm^{-3}. This systematic effect could be the result of a calibration issue, or possibly a slight density gradient in the $\hat{\mathbf{z}}$-direction (as the interferometer was nearly 3 m closer to the cathode than the langmuir probe was). The ion temperature was estimated to be approximately 1.25 eV based on previous interferometric measurements in a similar plasma, although no ion temperature measurement was available at the time our experiments were performed. The resulting ratio $v_{te}/v_A = 1.8$ places our experiments in the kinetic regime.

For the inertial regime, a higher magnetic field and lower electron density and temperature were desired so that $v_{te}/v_A < 1$. In order to achieve this, an axial magnetic field of 2300 G was applied, and experiments were conducted during the afterglow (the peroid after the discharge has ended, here approximately 920 μs after the end of the discharge). In the afterglow, electron density and temperature decrease rapidly, reducing the ratio v_{te}/v_A. Experiments were performed at a point in the afterglow when the electron density was 6.5×10^{11} cm^{-3} (after the 14% decrease) and the electron temperature was 1.9 eV. Just as in the kinetic experiments, the ion temperature was estimated to be approximately 1.25 eV. The resulting ratio $v_{te}/v_A = 0.18$ places these experiments in the inertial regime.

B. Antenna

Shear Alfvén waves were launched using an antenna inserted into the plasma with the axial magnetic field perpendicular to the antenna face shown in Figure 1. The antenna is composed of 48 copper-mesh elements, each extending approximately 30.5 cm in the vertical ($\hat{\mathbf{y}}$) direction. As a result, the wave field shows minimal vertical variation at the $\hat{\mathbf{y}}$ location of the wave measurements. The antenna elements are spaced by 0.635 cm in the $\hat{\mathbf{x}}$-direction. Each element is connected to its own independent signal driver, allowing control over the current supplied to each individual antenna element. A common signal is split and fed into each of the signal drivers, which then control the signal amplitude and phase (0° or 180°) as well as introduce a DC bias to each antenna element. The DC bias is used to ensure that the current on each antenna element is driven in a regime where the characteristic I-V curve of the plasma is linear, minimizing the amount of power that is deposited into harmonics of the fundamental driven frequency. This helps us to avoid signal rectification that results from trying to draw ion current. Control of the signal amplitude and phase allows a user to create a waveform along the $\hat{\mathbf{x}}$-axis with an arbitrary spatial structure, thereby controlling the structure of the perpendicular electric field of the wave. One of the primary advantages this antenna holds over antennas used in other dispersion experiments is that a user can control how power is distributed among perpendicular wave numbers, as seen in Figure 2. This figure shows the measured distribution of power as a function of $k_\perp$ for four different antenna patterns. This becomes particularly important when launching a wave with very small perpendicular structure. These waves are heavily damped, so putting most of the antenna power into a single high perpendicular wave number ensures that the signal will be strong enough to be detected several meters from the antenna. Experiments were performed using several different wave patterns, each of which covered a different subset of $k_\perp$ values. The results found while using these patterns were then superimposed in order to determine experimental dispersion and damping for a wide range of $k_\perp$.

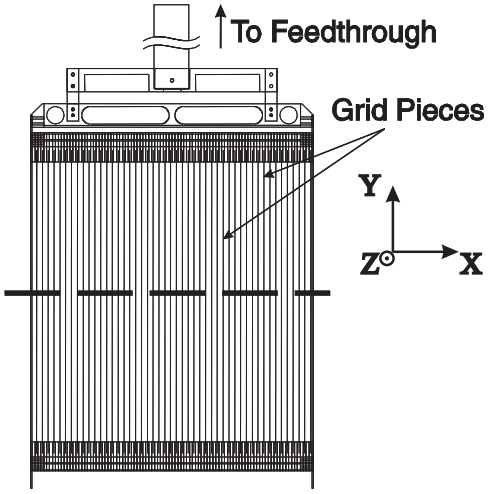

FIG. 1: This is a schematic view of the dispersive Alfvén wave antenna as seen along the z-axis of the LAPD. Each grid is made of copper mesh, and they are separated by 0.635 cm. Each grid may be driven separately, allowing good control over the perpendicular wave number. The dashed line shows the $\hat{x}$ and $\hat{y}$ positions at which raw data is acquired by b-dot probes placed at several $\hat{z}$ positions.

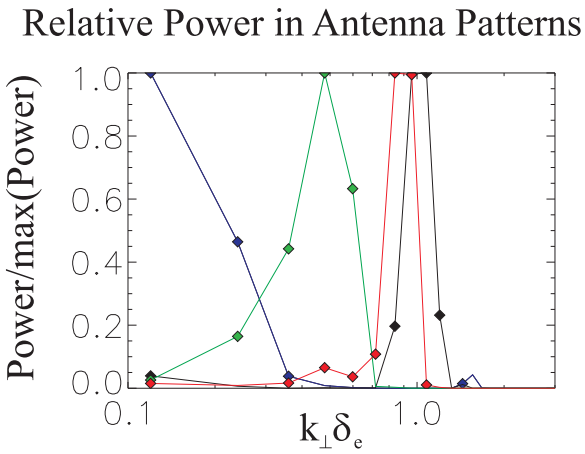

FIG. 2: (Color) This plot shows how the spatial perpendicular structure of the wave can be controlled by adjusting the antenna pattern. Measurements of the normalized power distribution as a function of $k_\perp$ is shown for the four different antenna patterns (represented by the four different colored lines) used in the inertial experiments.

The signal that was fed to the signal drivers was a limited-duration sinusoidal tone burst containing 5-10 periods of the wave and windowed temporally (the first and last signal peak were only half the amplitude of the rest of the signal). This temporal windowing was used to minimize the disturbance to the plasma due to the sudden presence of the wave. The wave frequency was set near 25% and 50% of the ion cyclotron frequency, resulting in wave frequencies of 70 kHz and 130 kHz in the kinetic regime (the ion cyclotron frequency was 229 kHz) and in the inertial regime, the wave frequencies were 250 kHz and 380 kHz (the ion cyclotron frequency was 876 kHz). This tone burst was then added to a DC bias that was chosen to maximize the amount of signal being driven at the fundamental frequency while minimizing the amount of power being deposited into harmonics due to current rectification in the sheath.

C. Data acquisition

Instead of measuring the predicted radial profile of the wave[16–19], in this analysis the wave is separated into $k_\perp$ components and the parallel phase velocity is determined for each component. The current analysis procedure is a refinement of the procedure used by Kletzing et al.[31] The ratios of v_{te}/v_A are more extreme than the intermediate regime presented in the earlier paper and our ability to launch and detect shear Alfvén waves has been significantly improved.

The waves were detected using three-axis magnetic search coil probes (or "B-dot" probes). These probes consist of 40 loops in each orthogonal direction, with a loop diameter of 1.2 mm. The probes also include an integrated amplifier circuit located on the probe head within the vacuum chamber, allowing us to amplify the relatively small signals before they are subjected to noise contamination on their path out of the vacuum chamber. Two probes were inserted into the plasma, separated by 1.92 m along the axis of the device (see Figure 3). An automated motion system was used to measure the wave at 181 horizontal ($\hat{\mathbf{x}}$) positions spaced by 2 mm across the diameter of the plasma and vertically located at the center of the plasma and antenna (see Figure 1).

At each spatial position, a time series was recorded at a sampling rate of 12.5 MHz. Since the plasma conditions were very reproducible between discharges on the LAPD, the signal-to-noise ratio was able to be increased through the averaging of multiple shots at each spatial position. Averaging 20-30 shots per spatial position provided a suitable signal-to-noise ratio for the purposes of this experiment. Figure 4 shows a plot of the $\hat{\mathbf{y}}$-component of the time-varying magnetic field as a function of position and time. Only the $\hat{\mathbf{y}}$-component of the wave magnetic field is shown since the wave electric field is almost completely in the $\hat{\mathbf{x}}$-direction, resulting in an almost purely B_y magnetic field.

In order to separate the wave into $k_\perp$ components, data like those shown in Figure 4 were passed through a spatial Fourier transform. This was done for the data measured at both axial probe positions. For each value of $k_\perp$, a time-series cut was taken from each probe location, an example of which is shown in Figure 5a. It can be seen that the signal received by the probe far from the antenna is smaller in amplitude and delayed in time with respect to the signal from the close probe. We made the assumption that the time and amplitude differences between the two received signals were due only to linear propagation and damping of the wave as it travels through the plasma. In the analysis, the phase velocity and damping factor of this wave were found by determining how much the lag and the amplitude of the far-probe signal would have to be adjusted in order to minimize the χ^2 value for the comparison of the two signals. Care was taken to correlate only the center sections of the two waves in order to ensure a measurement of the phase velocity rather than the group velocity corresponding to the envelope. The resulting correlated signals are shown in Figure 5b, with a plot of χ^2 and the correlation "R" value in Figure 5c as a function of lag. Using the best lag and amplitude adjustment as defined by the maximum of R and the minimum of χ^2, along with the probe separation and wave frequency, we calculated the parallel phase velocity $v_p = \omega/\mathrm{Re}(k_{||})$ as well as the damping factor $\mathrm{Im}(k_{||})/\mathrm{Re}(k_{||})$ for the selected value of $k_\perp$. This procedure was repeated for each value of $k_\perp$ in order to generate values of parallel phase velocity and damping as a function of $k_\perp$.

V. RESULTS

Results of kinetic Alfvén wave experiments are shown in Figures 6 and 7. Figure 6 shows plots of the normalized phase velocity (v_p/v_A) as a function of $k_\perp\rho_s$, while figure 7 show plots of the normalized damping factor ($\mathrm{Im}(k_{||})/\mathrm{Re}(k_{||})$) as a function of $k_\perp\rho_s$. The theoretical curves represent the results from using several different collisional models. The three black curves represent the results when collisions are neglected, with the center curve assuming the plasma properties reported in Section IV, and the two outer curves assuming random uncertainties in density, electron temperature, and magnetic field (3%, 10%, and 5% respectively for the kinetic case, and 5%, 7%, and 5% for the inertial case). The random uncertainties for the density and electron temperature were found by calculating the standard deviation of the plasma properties across the plasma diameter for the time at which experiments were conducted. All of the other curves represent the results from the various collisional models discussed earlier (according to the plot legend). Data points in these figures show the result of superimposing the data found from one (70 kHz case) or two (130 kHz case) different antenna patterns that were used to cover the $k_\perp$ spectra. Data points were only included for values of $k_\perp$ where the amplitude signal-to-noise ratio of the probe farthest from the antenna exceeded a value of 6, and the linear correlation value "R" exceeded a value of 0.9. The source of uncertainty in the data points arises from an uncertainty in the correlation process. The error bars are determined by scaling the χ^2 value so that the reduced-$\chi^2 = 1$, and then varying the lag and multiplicative factor independently to find the values of the lag and multiplicative factor that make χ^2 increase by 2.3, which corresponds to a 68.3% confidence interval (see p. 697 of Press et al.[32]) appropriate for a 1σ error.

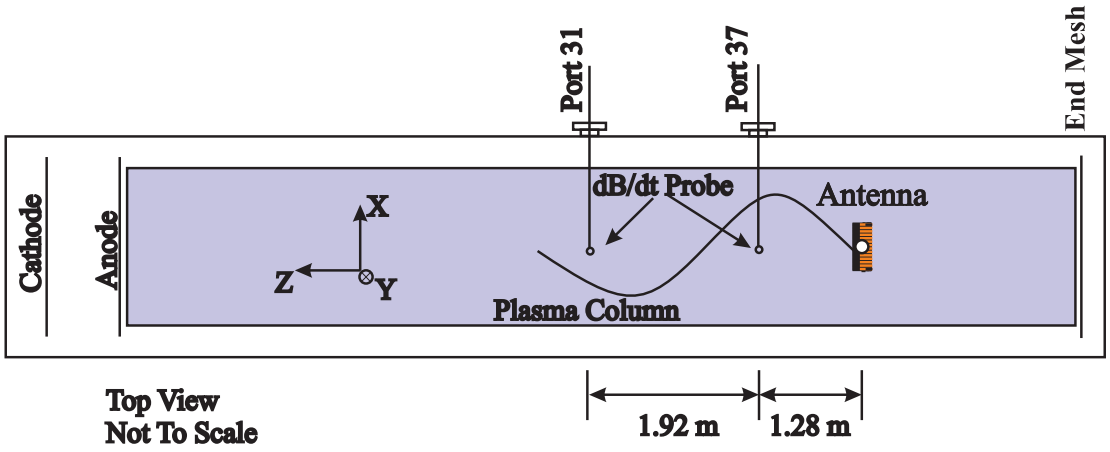

FIG. 3: (Color online) This schematic shows the placement of the b-dot probes with respect to the cathode and antenna. Waves are launched toward the cathode. The wave is then measured by two probes separated by a couple of meters.

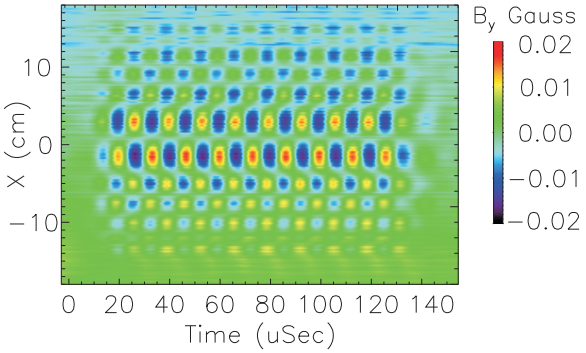

FIG. 4: (Color) The wave magnetic field (B_y) measured by the 'close' probe as a function of position across the plasma diameter and time. Data was sampled at 25 MHz and 8 shots were averaged together at each position to reduce noise.

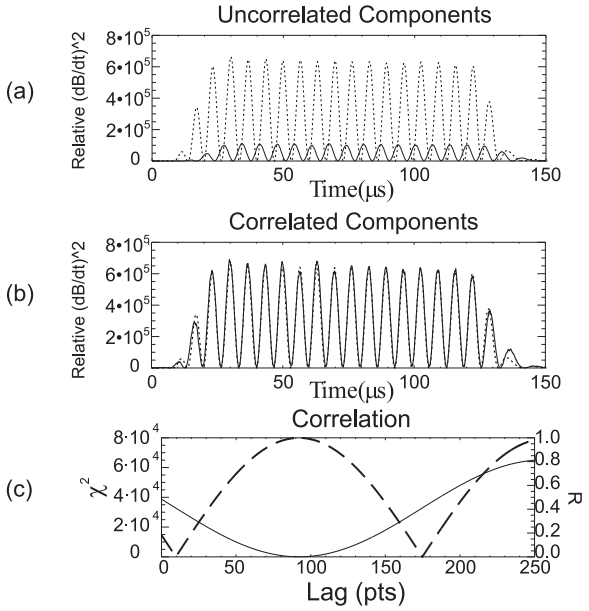

FIG. 5: (a) Signals from the probe closest to the antenna (dashed) and the probe further from the antenna (solid) before correlation has been performed. As expected, the far signal is seen at a later time and is smaller because it has been damped. (b) The result of the correlation technique where the far signal has been shifted in time and amplitude in order to best match the near signal. (c) Values of χ^2 (solid) and the correlation parameter R (dashed) as a function of signal 2 lag time. The 'best' lag and amplitude occur where χ^2 is minimized and R is maximized.

The first thing to notice in these plots is that the damping values predicted by all of the collisional models are significantly higher than the observed damping values. Not only are the damping values high, but there is also very little agreement between the collisional models, with the non-conserving Krook model showing the least agreement with experimental values. The best agreement for the kinetic results are when electron collisions are completely ignored and damping is purely Landau damping.

The inertial results are presented in Figures 8 and 9. As in the kinetic regime results, these figures show plots of the normalized phase velocity (v_p/v_A) and normalized damping factor ($\mathrm{Im}(k_{||})/\mathrm{Re}(k_{||})$), where $k_\perp$ is now normalized to the electron skin depth δ_e on the x-axis. In both the 250 kHz and 380 kHz cases, data points taken from 4 antenna patterns (seen in Figure 2) are superimposed in order to cover the $k_\perp$ range of interest.

Unlike in the kinetic regime, Landau damping alone fails to account for the observed wave damping in the inertial regime. Another important difference is that in the inertial regime, all three Krook collision models provide essentially the same dispersion and damping prediction over the range of $k_\perp$ for which we can compare to experimental values. The results from the inclusion of a Lorentz collision operator result in damping values between those predicted by Landau damping and the Krook collision values, and tends to be lower than the observed values. The phase velocity prediction from Lorentz damping is relatively close to the predictions from the Krook operators, and falls within error bars of the observed values.

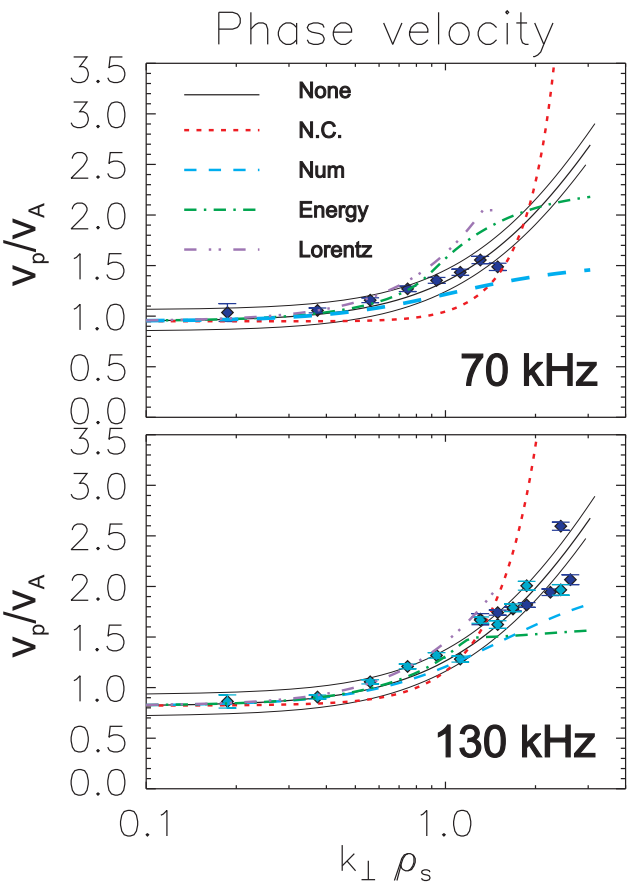

FIG. 6: (Color) Kinetic Alfvén wave parallel phase velocity measurements compared to warm plasma theory for (a) 70 kHz ($.3\omega_{ci}$) and (b) 130 kHz ($.57\omega_{ci}$). The effects of different models for electron collisions are represented according to the legend. Convergence issues prevent the curve arising from the use of the Lorentz operator from being extended much beyond $k_\perp \rho_s = 1$ for these plasma parameters.

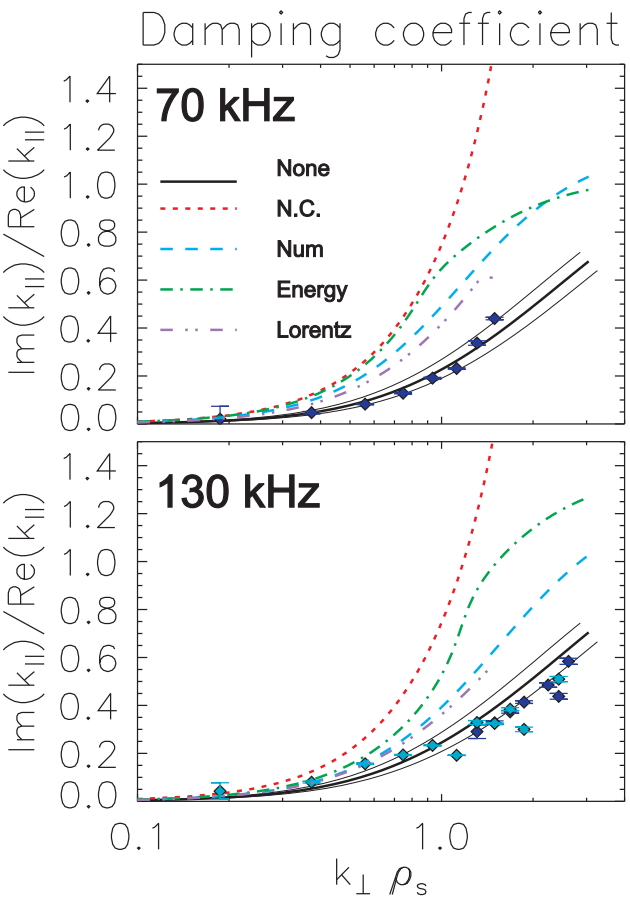

FIG. 7: (Color) Kinetic Alfvén wave damping measurements compared to warm plasma theory for (a) 70 kHz ($.3\omega_{ci}$) and (b) 130 kHz ($.57\omega_{ci}$).

VI. DISCUSSION

Results from the kinetic and inertial regimes show very different behaviors with respect to collisionality. When electron collisions are included in the Boltzmann equation for the kinetic regime, the resulting theoretical phase velocity shows very little agreement with the observed phase velocity, and the theoretical damping factor is much larger than observed values. This shows that the collision operators examined in this paper tend to overestimate the effect of electron collisions for this wave mode. Additionally, there is not much agreement in the damping values predicted by the different collision operators in this regime, nor even an obvious trend as the complexity of the collision operator increases. In order to best match the experimentally observed values, electron collisions must be completely neglected.

In contrast, it is essential to include electron collisional effects to describe wave behavior in the inertial regime. Landau damping alone predicts far less damping than what is observed. Additionally, higher phase velocities are predicted when collisionality is neglected. In the inertial regime, there is also far better agreement between the predictions of the collisional models. In fact, the phase velocity and damping predictions from the Krook models nearly overlap each other (as well as the data) over the range of $k_\perp$ values for which we have measurements. It should be noted that the prediction from the Lorentz collision operator does not agree with the observed values or the Krook predictions for the inertial case.

Focusing first on the comparison of experimental values to the predictions from Krook operators, it is clear that the Krook model does a better job predicting the dispersion and damping of the wave in the inertial regime than it does in the kinetic regime. However, the physical reasoning behind this difference is not completely understood. One possibility is that the kinetic regime experiments were conducted in a parameter regime in which the Krook collision operator is not well suited to describing collisions effectively. Electron-ion collisions are not isotropic in the presence of a magnetic field, with the parallel collision frequency multiplied by a factor of 0.51 with respect to the perpendicular collision frequency (taken as ν_{ei}) in many two-fluid treatments (e.g. Braginskii[1]). Even if this factor of two were included in all three directions, it still does not change the theoretical curves enough to match

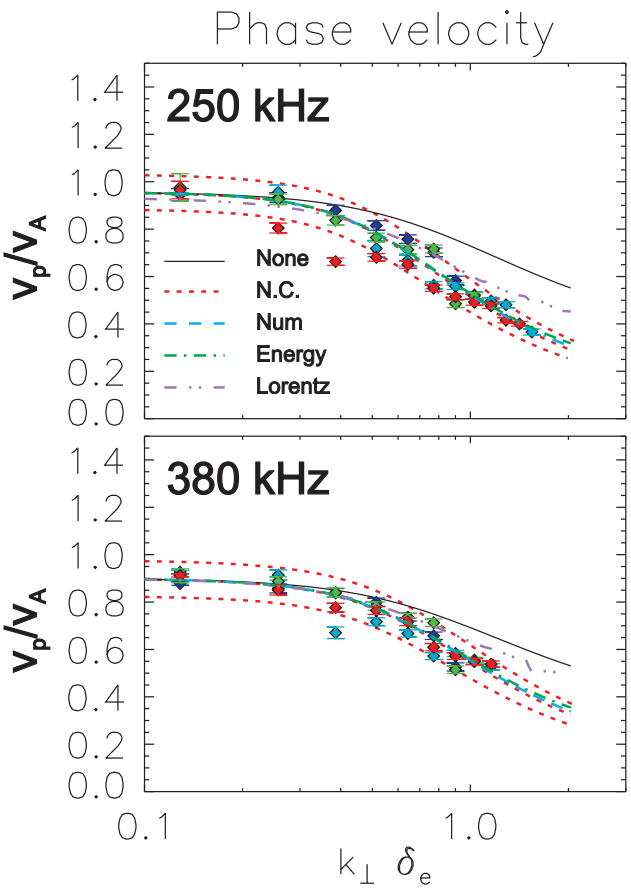

FIG. 8: (Color) Inertial Alfvén wave parallel phase velocity measurements compared to warm plasma theory for (a) 250 kHz ($.29\omega_{ci}$) and (b) 380 kHz ($.43\omega_{ci}$). Note the extremely good agreement between the three Krook operator results.

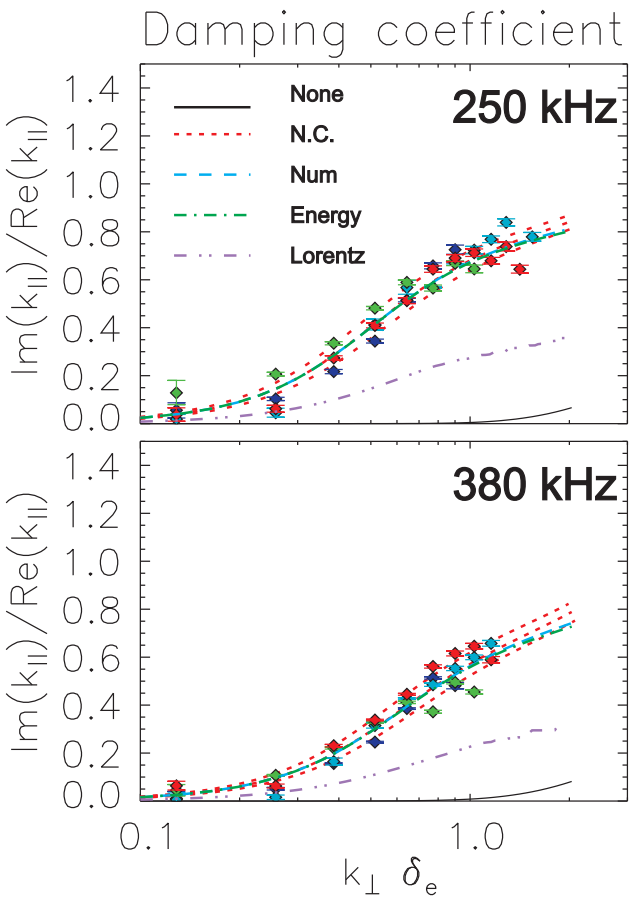

FIG. 9: (Color) Inertial Alfvén wave damping measurements compared to warm plasma theory for (a) 250 kHz ($.29\omega_{ci}$) and (b) 380 kHz ($.43\omega_{ci}$). Note the extremely good agreement between the three Krook operator results.

experimental results in the kinetic regime.

Instead, we suspect the above difference to be related to the difference in the electron physics in the kinetic and inertial regimes. Electrons are relatively hotter and respond differently to the wave in the kinetic regime than in the inertial regime. In the kinetic regime, $v_{te} > v_A$. This means that from the electron frame, the electric field of the wave appears quasi-static. The electrons are able to thermalize quickly in the presence of this wave electric field and are effectively an equilibrium distribution. This is basically the same reasoning presented by Goertz and Boswell[12] when they assume that in the kinetic regime, the electrons react rapidly to the changing parallel electric field E_z, resulting in a Boltzmann electron distribution. Since the electrons are already in a Boltzmann distribution, the role of electron collisions in Equation 4 becomes negligible.

In the inertial regime, the cold electrons are treated as a cold fluid. So, as the shear Alfvén wave passes, the distribution "sloshes" back and forth due to the time-varying wave electric field uniformly accelerating all electrons in the distribution. Since the acceleration of the ions by the parallel wave electric field will be opposite that of the electrons, collisions between electrons and ions impede this sloshing of the distributions. Additionally, since the electrons are relatively cold, they are unable to thermalize quickly in the absence of electron-electron collisions in the event that the electron distribution departs from a Boltzmann distribution. Under these conditions, the importance of electron collisions increases in the Krook collision term of Equation 4. This could explain why electron collisions are absolutely necessary for good agreement in the inertial regime, but must be neglected in the kinetic regime. Work is being done to quantitatively include this qualitative argument into the warm-plasma theory.

A first attempt to include particle velocity dependency into the description of electron collisions included a modification $Z'(\zeta) \rightarrow Z_P(\zeta)$ in the parallel dielectric tensor element ε_{zz} in order to include effects of pitch-angle scattering of electrons off ions. Pitch-angle scattering incorporated through the use of the Lorentz collision operator failed to agree with the observed dispersion and damping values in either regime. In both cases, the predicted damping values lie between those predicted by Krook collisions and those predicted in the Landau damping case. As such, the damping predictions are closer than those given by the Krook models in the kinetic regime, but the opposite is true in the inertial regime. Hedrick

et al.[7] points out that one deficiency of the Lorentz collisional model is that it does not include energy scattering like the Krook models do. The Lorentz collisional model also only addresses electron-ion collisions, ignoring the effect of electron-electron collisions. As such, it may be possible that the Lorentz operator may be as bad (in the kinetic regime), or even worse (in the inertial regime), than the conserving Krook operators in describing electron collisions, even though it has the advantage of a velocity-dependent collision frequency. Additionally, to our knowledge, no formal derivation exists showing that the substitution $Z(\zeta) \rightarrow Z_P(\zeta)$ by Peñano et al.[29] is valid in the purely damping case.[5] It should also be noted that the Lorentz operator represents collisions between electrons and ions as being elastic. In reality, though, it is natural to expect that these collisions may instead be inelastic due to radiated power losses.

VII. CONCLUSIONS

We have presented measurements of parallel phase velocity and damping as a function of $k_\perp$ for a shear Alfvén wave in the kinetic and inertial regimes that allow us to test models of electron collisions. Measurements were compared to warm plasma theory with several different collisionality cases. Theoretical curves were found using several collisional models to describe electron collisions, as well as curves found in the collisionless case. In the kinetic regime, good agreement was found between experiment and the collisionless case, while it was necessary to include electron collisions via a Krook collision operator to see the same level of agreement with experiment in the inertial regime. Physically, we believe this difference arises due to the fundamentally different response of the electron distribution function to the presence of the wave in the two shear Alfvén wave regimes.

Acknowledgments

Funding was provided by NSF Grant No. ATM 03-17310 and DOE Grant No. DE-FG02-06ER54890. The experiments presented here were conducted at the Basic Plasma Science Facility, which is funded by the U.S. Department of Energy and the National Science Foundation. The authors would like to thank W. Gekelman, W. Daughton, and A. Bhattacharjee for helpful discussions.

This work is part of a dissertation to be submitted by D. J. Thuecks to the Graduate College, University of Iowa, Iowa City, IA, in partial fulfillment of the requirements for the Ph.D. degree in physics.

* Electronic address: derek-thuecks@uiowa.edu

[1] S. I. Braginskii, Rev. Plasma Phys. **1**, 205 (1965).
[2] E. P. Gross, Phys. Rev. **82**, 232 (1951).
[3] P. L. Bhatnagar, E. P. Gross, and M. Krook, Phys. Rev. **94**, 511 (1954).
[4] E. P. Gross and M. Krook, Phys. Rev. **102**, 593 (1956).
[5] M. Opher, G. J. Morales, and J. N. Leboeuf, Phys. Rev. E **66**, 016407 (2002).
[6] G. Rewoldt, W. M. Tang, and R. J. Hastie, Phys. Fluids **29**, 2893 (1986).
[7] C. L. Hedrick, J.-N. Leboeuf, and D. A. Spong, Phys. Plasmas **2**, 2033 (1995).
[8] W. Gekelman, H. Pfister, Z. Lucky, J. Bamber, D. Leneman, and J. Maggs, Rev. Sci. Instrum. **62**, 2875 (1991).
[9] H. Alfvén, Nature **150**, 405 (1942).
[10] R. J. Stéfant, Phys. Fluids **13**, 440 (1970).
[11] A. Hasegawa, J. Geophys. Res. **81**, 5083 (1976).
[12] C. Goertz and R. Boswell, J. Geophys. Res. **84**, 7239 (1979).
[13] C. Kletzing and S. Hu, Geophys. Res. Lett. **693**, 4 (2001).
[14] R. C. Cross, Plasma Phys. **25**, 1377 (1983).
[15] G. G. Borg, M. H. Brennan, R. C. Cross, L. Giannone, and I. J. Donnelly, Plasma Phys. Controlled Fusion **27**, 1125 (1985).
[16] W. Gekelman, S. Vincena, D. Leneman, and J. Maggs, J. Geophys. Res. **102**, 7225 (1997).
[17] W. Gekelman, J. Geophys. Res. **104**, 14417 (1999).
[18] D. Leneman, W. Gekelman, and J. Maggs, Phys. Plasmas **7**, 3934 (2000).
[19] S. Vincena, W. Gekelman, and J. Maggs, Phys. Plasmas **8**, 3884 (2001).
[20] G. J. Morales, R. S. Loritsch, and J. E. Maggs, Phys. Plasmas **1**, 3765 (1994).
[21] G. Morales and J. Maggs, Phys. Plasmas **4**, 4118 (1997).
[22] D. Swanson, *Plasma Waves* (Institute of Physics Publishing, Bristol and Philadelphia, 2003), 2nd ed.
[23] B. D. Fried and S. D. Conte, *The Plasma Dispersion Function* (Academic Press: New York, 1961).
[24] B. B. Kadomtsev, *Plasma turbulence* (Academic Press, New York, 1965).
[25] P. Clemmow and J. Dougherty, *Electrodynamics of Particles and Plasmas* (Addison-Wesley, London, 1969).
[26] B. D. Fried, A. N. Kaufman, and D. L. Sachs, Phys. Fluids **9**, 292 (1966).
[27] A. Alexandrov, L. Bogdankevich, and A. Rukhadze, *Principles of Plasma Electrodynamics* (Springer-Verlag, New York, 1984).
[28] R. A. Koch and W. Horton, Jr., Phys. Fluids **18**, 861 (1975).
[29] J. R. Peñano, G. J. Morales, and J. E. Maggs, Phys. Plasmas **7**, 144 (2000).
[30] P. Helander and D. J. Sigmar, *Collisional transport in magnetized plasmas* (Cambridge University Press, Cambridge, U.K., 2002).
[31] C. Kletzing, S. Bounds, and J. Martin-Hiner, Phys. Rev. Lett. **90** (2003).
[32] W. H. Press, S. A. Teukolsky, W. T. Vetterling, and B. P. Flannery, *Numerical recipes in C (2nd ed.): the art of scientific computing* (Cambridge University Press, New York, NY, USA, 1992), ISBN 0-521-43108-5.